Meteorol. Atmos. Phys. 73, 1–23 (2000)

Meteorology and Atmospheric Physics

[1] Department of Astronomy and Meteorology, Faculty of Science, Cairo University, Cairo, Egypt
[2] Department of Astronomy and Meteorology, Faculty of Science, Al-Azhar University, Nasr City, Cairo, Egypt

Energy Exchanges for Mediterranean Weather Systems

M. Abdel Wahab[1] and **H. Abdel Basset**[2]

With 11 Figures

Received July 2, 1998
Revised December 28, 1998

Summary

An analysis of the kinetic energy budget is made for a cyclonic development over the Mediterranean. Horizontal flux convergence constitutes a major energy source. Generation of kinetic energy via cross-contour flow is a persistent sink except only a weak energy source for the decay period of our case study. Dissipation of kinetic energy, computed as a residual, has local maxima both in the lower troposphere and near the jet stream level. By investigating the relative importance of divergent and non-divergent components in the kinetic energy budget we found that when calculating the magnitude of the kinetic energy one may safely replace the total wind with the non-divergent one. But the horizontal flux convergence of kinetic energy and the generation of kinetic energy are sensitive to the magnitude of the divergent wind.

A large increase in the kinetic energy of the total flow fields and the nondivergent component of the flows occurs over the southeastern Mediterranean with the existence of the subtropical jet. This indicates that the subtropical jet steadily receives energy from divergent flow. Maximum energy conversion and transport occur near the time of maximum storm intensity while smaller values are observed during the development and decay stages.

1. Introduction

Relatively few studies as applied to convectively unstable synoptic situations. Synoptic-scale kinetic energy analysis have shown convective storm environments to be regions of intense energy transformations and transports (Fuelberg and Scoggins, 1978; Robertson and Smith, 1980). Widespread convection is thought to be a source of synoptic-scale kinetic energy (Vincent and Schlatter, 1979) due to transfer of unresolvable (subgrid) to resolvable (grid) scales of motion (Kung, 1969; Smith, 1973; Smith and Adhikary, 1974). Sources and sinks of kinetic energy within the mesoscale storm environment appear to be more intense that those at the larger scales (McInnis and Kung, 1972; Kung and Tsui, 1975; Tsui and Kung, 1977; Fuelberg and Jedlovec, 1982).

A different approaches for describing kinetic energy balance is to consider the relative contributions of the divergent and rotational wind components. Using northern Hemispheric summer time data, Chen and Wiin-Nielsen (1976) found that the ratio of divergent kinetic energy to the total amount is approximately 0.10. In other words, the rotational wind is the dominant component of 200 mb tropical flow (Krishnamurti, 1971; Chen, 1980). Although it was small in magnitude, the divergent wind assumed crucial importance in the generation and transport of kinetic energy within a midlatitude cyclone (Chen et al., 1978). Similarly kinetic energy of the Arabian Sea monsoon was observed to increase via interactions between the divergent and rotational wind components (Krishnamurti and Ramanathan, 1982). On the other hand, much of the cross contour generation

of kinetic energy in some cyclones has been attributed to the rotational wind (Kristnamurti, 1968; DiMego and Bosart, 1982).

The purpose of the present study is to discuss and analyze the kinetic energy budget of a developing cyclone over a limited area in the mid-latitude during 23 February to 10 March 1987. Also, to examine the relative contributions of the divergent and nondivergent wind components to the kinetic energy budget. Finally, we will illustrate the major role of the transfer of energy from the divergent to the rotational components.

2. Theoretical Consideration

2.1 The Kinetic Energy Equation

In pressure coordinates, the rate of change of kinetic energy in an atmospheric column is

$$\begin{aligned}\frac{\partial K}{\partial t} &\equiv \frac{1}{sg}\int_0^{P_0}\int_S \frac{\partial k}{\partial t}\,dsdP \\ &= -\frac{1}{sg}\int_0^{P_0}\int_S \nabla\cdot(Vk)dsdP \\ &\quad -\frac{1}{sg}\int_0^{P_0}\int_S \frac{\partial(\omega k)}{\partial P}\,dsdP \\ &\quad -\frac{1}{sg}\int_0^{P_0}\int_S V\cdot\nabla\phi\,dsdP - D(k), \qquad (1)\end{aligned}$$

where S is the area of computational domain, g is the acceleration due to the gravity and P_0 is the surface pressure. On the right-hand side of (1), the first and second terms are the horizontal and vertical flux divergence of kinetic energy, the third term is the generation of kinetic energy due to the cross-contour flow and the last term $D(k)$, commonly called the ''dissipation'' term.

To examine contributions of the divergent and rotational winds to the total kinetic energy balance, these components must be introduced into (1). This can be done by following the procedure of Chen et al. (1978).

Helmholtz's theorem states that horizontal wind can be expressed as the sum of the divergent (V_D) and nondivergent (or rotational) components (V_R), i.e.,

$$V = V_R + V_D. \qquad (2)$$

The kinetic energy per unit mass can be expressed as

$$K = \frac{1}{2}V\cdot V = K_R + K_D + V_R\cdot V_D \qquad (3)$$

where

$$K_R = \frac{1}{2}V_R\cdot V_R \quad \text{and} \quad K_D = \frac{1}{2}V_D\cdot V_D. \qquad (4)$$

Using (2), we may write the integrands of the first and third terms on the right-hand side of (1) as

$$-\nabla\cdot(VK) = -V\cdot(V_R K) - \nabla\cdot(V_D K), \qquad (5)$$

$$-V\cdot\nabla\phi = -V_R\cdot\nabla\phi - V_D\cdot\nabla\phi. \qquad (6)$$

Equation (5) shows that the horizontal flux convergence of kinetic energy is caused by the horizontal transport of nondivergent and divergent winds. For sake of convenience we associate $-V_R\nabla\phi$ and $-V_D\nabla\phi$ with the generation of kinetic energy due to barotropic and baroclinic proceses, respectively (Pearce, 1974; Chen and Wiin-Nielson, 1976). The barotropic term integrates to zero in a closed domain (Chen and Wiin-Nielson, 1976), but not in an open domain as considered here. Using (5) and (6), we can rewrite (1) as

$$\begin{aligned}\frac{1}{sg}\int_0^{P_0}\int_S \frac{\partial k}{\partial t}\,dsdP &= -\frac{1}{sg}\int_0^{P_0}\int_S \nabla\cdot(V_R k)dsdP \\ &\quad -\frac{1}{sg}\int_0^{P_0}\int_S \nabla\cdot(V_D k)dsdP \\ &\quad -\frac{1}{sg}\int_0^{P_0}\int_S \frac{\partial(\omega k)}{\partial P}\,dsdP \\ &\quad -\frac{1}{sg}\int_0^{P_0}\int_S V_R\cdot\nabla\phi\,dsdP \\ &\quad -\frac{1}{sg}\int_0^{P_0}\int_S V_D\cdot\nabla\phi\,dsdP - D(k). \qquad (7)\end{aligned}$$

We shall pay particular attention to the contribution of V_R and V_D to kinetic energy in (3), to the horizontal flux onvergence of kinetic energy $-\nabla\cdot(Vk)$ in (5), and to the generation of kinetic energy $-V\cdot\nabla\phi$ in (6).

2.2 $\psi\cdot\chi$ Interactions

The conventional breakdown of the horizontal wind V_H into irrotational and nondivergent

components (Eq. 2) can be also expressed by the relations

$$V_H = V_\psi + V_\chi, \tag{8.1a}$$

$$V_\psi = K \times \nabla\psi, \tag{8.1b}$$

$$V_\chi = -\nabla\chi \,(\text{Note the sign}), \tag{8.1c}$$

$$\nabla \cdot V_H = -\nabla^2\chi, \tag{8.1d}$$

$$K \cdot \nabla \times V_H = \nabla^2\psi. \tag{8.1e}$$

Here ψ is the streamfunction and χ is the velocity potential. The energy equations in terms of these components are usually expressed by the relations (Krishnamurti et al., 1982).

$$\begin{aligned}\frac{\partial}{\partial t}K_\psi &= \nabla\cdot\psi\nabla\frac{\partial\psi}{\partial t} - \psi\nabla\cdot f\nabla\chi \\ &- \psi\nabla\chi\cdot\nabla(\nabla^2\psi) - \psi\nabla^2\chi\nabla^2\psi \\ &+ \psi\omega\frac{\partial}{\partial P}\nabla^2\psi + \psi\nabla_{\omega\cdot}\nabla\frac{\partial\psi}{\partial P} \\ &- \psi J\left(\omega,\frac{\partial\chi}{\partial P}\right) + \psi J(\psi,\nabla^2\psi + f) + F_\psi,\end{aligned} \tag{9}$$

$$\begin{aligned}\frac{\partial}{\partial t}K_\chi &= \nabla\cdot\chi\nabla\frac{\partial\chi}{\partial t} - \chi\nabla^2\phi + \chi\nabla\cdot f\nabla\Psi \\ &+ \chi(\nabla^2\psi)^2 - \chi\nabla^2(\nabla\psi)^2/2 - \chi\nabla^2(\nabla\chi)^2/2 \\ &+ \chi\nabla\psi\cdot\nabla(\nabla^2\psi) - \chi\omega\frac{\partial}{\partial P}\nabla^2\chi + \chi\nabla\omega\cdot\nabla\frac{\partial\chi}{\partial P} \\ &+ \chi J\left(\omega,\frac{\partial\psi}{\partial P}\right) + \chi\nabla^2 J(\psi,\chi) - \chi J(f,\chi) \\ &+ \chi J(\chi,\nabla^2\psi) + F_\chi.\end{aligned} \tag{10}$$

Upon integration of the above equations over a horizontal domain and some rearrangement of terms, one can express the energy equation for the domain nondivergent and irrotational components by the relations:

$$\begin{aligned}\frac{\partial}{\partial t}\overline{\overline{K_\psi}} &= B_\psi + \overline{\overline{f\nabla\psi\cdot\nabla\chi}} + \overline{\overline{\nabla^2\psi\nabla\psi\cdot\nabla\chi}} \\ &+ \overline{\overline{\nabla^2\chi(\nabla\psi)^2/2}} + \overline{\overline{\omega J\left(\psi,\frac{\partial\chi}{\partial P}\right)}} + \overline{\overline{F_\psi}},\end{aligned} \tag{11}$$

$$\begin{aligned}\frac{\partial}{\partial t}\overline{\overline{K_\chi}} &= B\chi - \overline{\overline{\chi\nabla^2\phi}} - \overline{\overline{f\nabla\psi\cdot\nabla\chi}} \\ &- \overline{\overline{\nabla^2\psi\nabla\psi\cdot\nabla\chi}} - \overline{\overline{\nabla^2\chi(\nabla\psi)^2/2}} \\ &- \overline{\overline{\omega J\left(\psi,\frac{\partial\chi}{\partial P}\right)}} + \overline{\overline{F_\chi}}.\end{aligned} \tag{12}$$

Here B_ψ and B_χ denote boundary fluxes and the terms on the right-hand side with double overbars denote the $\psi\cdot\chi$ interactions. An equation for the time rate of change of internal plus potential energy over a closed domain may be expressed by a similar relation (Krishnamurti et al., 1982).

$$\frac{\partial}{\partial t}\overline{\overline{P+I}} = B_{P+I} + \overline{\overline{\chi\nabla^2\phi}} + \overline{\overline{G_{P+I}}} + \overline{\overline{D_{P+I}}}, \tag{13}$$

where B_{P+I} denotes a boundary flux term, and **G** and **D** denote the generation and dissipation terms, respectively.

For a closed system (i.e., $\mathbf{B}=0$), in the absence of heating friction, the sum of static plus kinetic energies of irrotational and nondivergent motion is an invariant. The conversion of static energy into kinetic energy of divergent motions is represented by $\overline{\overline{\chi\nabla^2\phi}}$. Since

$$\begin{aligned}\overline{\overline{\chi\nabla^2\phi}} &= \overline{\overline{\phi\nabla^2\chi}} = \overline{\overline{-\phi\frac{\partial\omega}{\partial P}}} = \overline{\overline{\omega\frac{\partial\phi}{\partial P}}} = \overline{\overline{-\omega\alpha}} \\ &= -\overline{\overline{\frac{R}{P}\omega T}},\end{aligned} \tag{14}$$

it denotes the ascent of relatively warm air and the descent of relatively colder air within the domain. It is interesting to note that the total kinetic energy of the nondivergent motions $\overline{\overline{K_\psi}}$ can only increase (in a closed domain) via $\psi\cdot\chi$ interactions. In the absence of $\psi\cdot\chi$ interaction and dissipation in the domain-averaged kinetic energy of nondivergent motion is conserved, as is the case of the barotropic nondivergent dynamics. If we were examining the energy transformations for a zonally symmetric model (formulated without any eddy flux parameterizations) then it can be shown that if the energy exchanges $\overline{\overline{-\omega T/P} > 0}$, it drives meridional (Hadley type) circulations, while the zonal circulations can only receive energy from the meridional motion via the effects of the earth's rotation. In the more general three-dimensional problem it is interesting to note that $\overline{\overline{-\omega T/P} > 0}$ has an analogous role, namely that it supplies energy to drive divergent circulations (Hadley as well as east-west) while the nondivergent circulation can only receive energy from the divergent motions. Differential heating (i.e., a covariance of heating and temperature) define the generation terms $\overline{\overline{G_{P+I}}}$, which can enhance the

internal plus potential energy; this energy can be released via instabilities and the attendant vertical overturnings, $\overline{\overline{-\omega T/P}}$.

We shall next examine the $\psi \cdot \chi$ interactions. The magnitude of the term $f\nabla\psi \cdot \nabla\chi$ depends on the orientation of the vectors $\nabla\psi$ and $\nabla\chi$. If over the Northern Hemisphere they are nearly parallel, i.e., $\nabla\psi \cdot \nabla\chi > 0$, then energy exchanges go from the irrotational to the nondivergent modes. A similar argument holds for the second term $\nabla^2\psi\nabla\psi \cdot \nabla\chi$ over regions of cyclonic vorticity over the Northern Hemisphere, while an opposing argument occurs for the Southern Hemisphere. This converse argument also holds for antiparallel vector, i.e., $\nabla\Psi \cdot \nabla\chi < 0$. The third term in this sequence $\nabla^2\psi\nabla\psi \cdot \nabla\chi/2$ expresses another kind of $\psi \cdot \chi$ interaction where the covariance of the horizontal divergence and the kinetic energy of the nondivergent component is important. At a single point the contribution of this term alone has the form, $\partial/\partial t(\nabla\psi \cdot \nabla\chi/2) = \nabla^2\psi\nabla\psi \cdot \nabla\chi/2$ and leads to an exponential growth of the nondivergent kinetic energy wherever the horizontal convergence $(\nabla^2\chi > 0)$ is positive. The last term in this sequence, i.e., $\omega J(\psi, \partial\chi/\partial P)$ defines a simple interpretation. Regions of large $\partial\chi/\partial P$ are generally also associated with regions of large vertical variations of convergence, i.e, $\partial\chi/\partial P \approx \partial/\partial P\nabla^2\chi$. Following the streamfunctions, downstream from these regions energy exchange from irrotational to the nondivergent flows can occur if there is general upward motion. The converse holds for the case upstream of these regions.

3. Data and Computation

3.1 Input Data

The data used in this study have been taken from the archives of the European center for Medium Range Forecasts (ECMRF). It consist of the horizontal wind components (u-eastward, v-northward), the temperature (T) and the geopotential height (z) on regular latitude-longitude grid points resolution of 2.5°×2.5°. The available data is only at 0000 GMT during the period 15 February to 11 March 1987 for isobaric levels 1000, 850, 700, 500, 300, 200 and 100 mb.

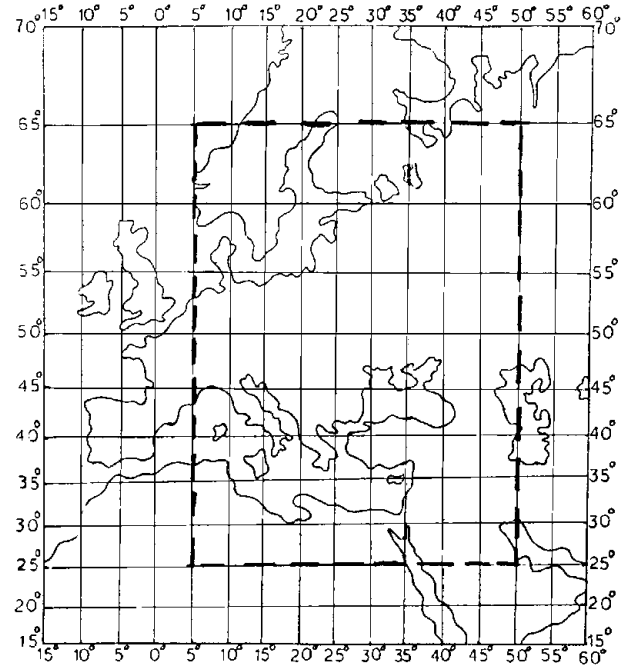

Fig. 1. The inner domain which is used for the kinetic energy budget calculations

Figure 1 shows the domain of the study which extends from 5.0° to 70.0° N and from 32.2° W to 70.0° E. The 1200 GMT was not available for the present study. The inner domain which is used for present case of study (Fig. 1) extends from 5° E to 55° E and from 25° N to 65° N, and the calculations of kinetic energy budget are made over this subdomain from 23 February to 10 March.

3.2 Analytical Procedures

The vertical wind component in the P-coordinate system, namely $\omega = dp/dt$, is estimated using the kinematic method. However, due to errors in horizontal divergence estimates, accumulation of error in ω occurs away from the bottom of the atmosphere. To remove this bias a pressure-weighted correction for ω was adopted following O'Brien (1970). This technique was employed to calculate grid point values of ω at all standard isobaric levels and at the midpoint of each sublayer. At the bottom and the top of the atmosphere ω was initially set to zero.

An advanced technique for obtaining divergent and nondivergent winds (V_R and V_D) is the solution of poisson equations for stream function

and velocity potential using the relaxation method (Krishnamurti and Bounoua, 1996). The energy variables are calculated at 0000 GMT. Therefore, time derivatives evaluated by central differences spanning of 48 h give a reasonable indication of the time variation of kinetic energy Centered finite differences were used to compute horizontal derivatives and all vertical derivatives except those at the 1000 and 100 mb, where noncentered differences were employed. For each of wind analysis at 1000 mb, energy variables at this level are obtained by linear extrapolation. Finally, the dissipation term is evaluated as a residual in Eq. (1) (Kung, 1966). Holopainen (1973) warms of the risk in attaching physical significance to the sign or magnitude of residual terms, but concedes that application of the residual technique may be meaningful in data-rich areas.

4. Synoptic Discussion

A common case of winter cyclogenesis over the Mediterranean is considered in the present study. Its period embraces the last week of February and the first 10 days of March 1987. Based on the surface charts, changes in central pressure and charts of 500 mb the life cycle of this cyclone (case of study) can be divided as following:

Per-storm period:	–0000 GMT 23 February
	– 0000 GMT 26 February
Growth period:	0000 GMT 27 February
	– 000 GMT 4 March
Decay period:	0000 GMT 5 March
	– 000 GMT 10 March.

Surface and 500 mb charts at 0000 GMT on each day are shown in Figs. 2 and 3, respectively. Surface charts depict isobars of sea level pressure with five millibar increments and surface fronts.

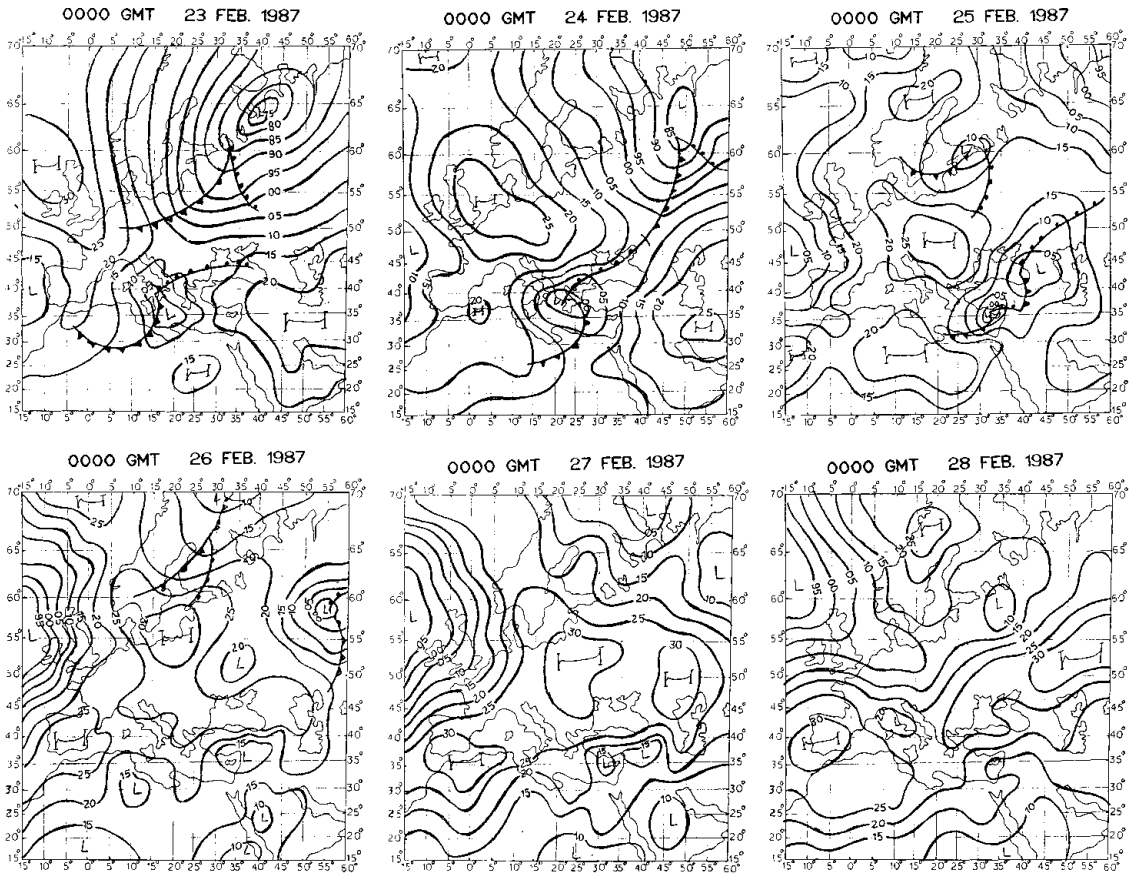

Fig. 2a. Sea level isobars in 5 mb increments and surface fronts for 0000 GMT 23 February to 10 March, 1987

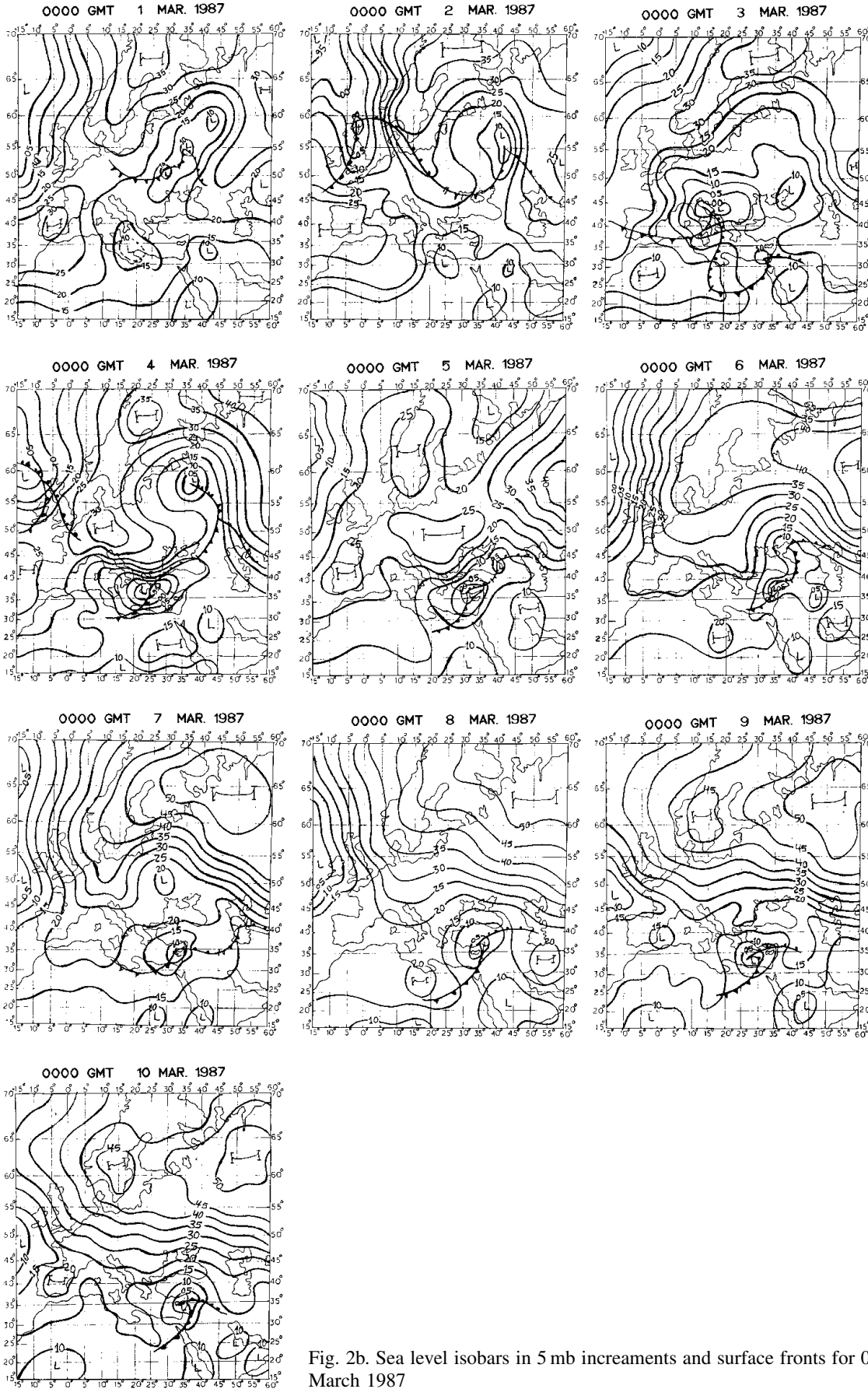

Fig. 2b. Sea level isobars in 5 mb increaments and surface fronts for 0000 GMT 1–10 March 1987

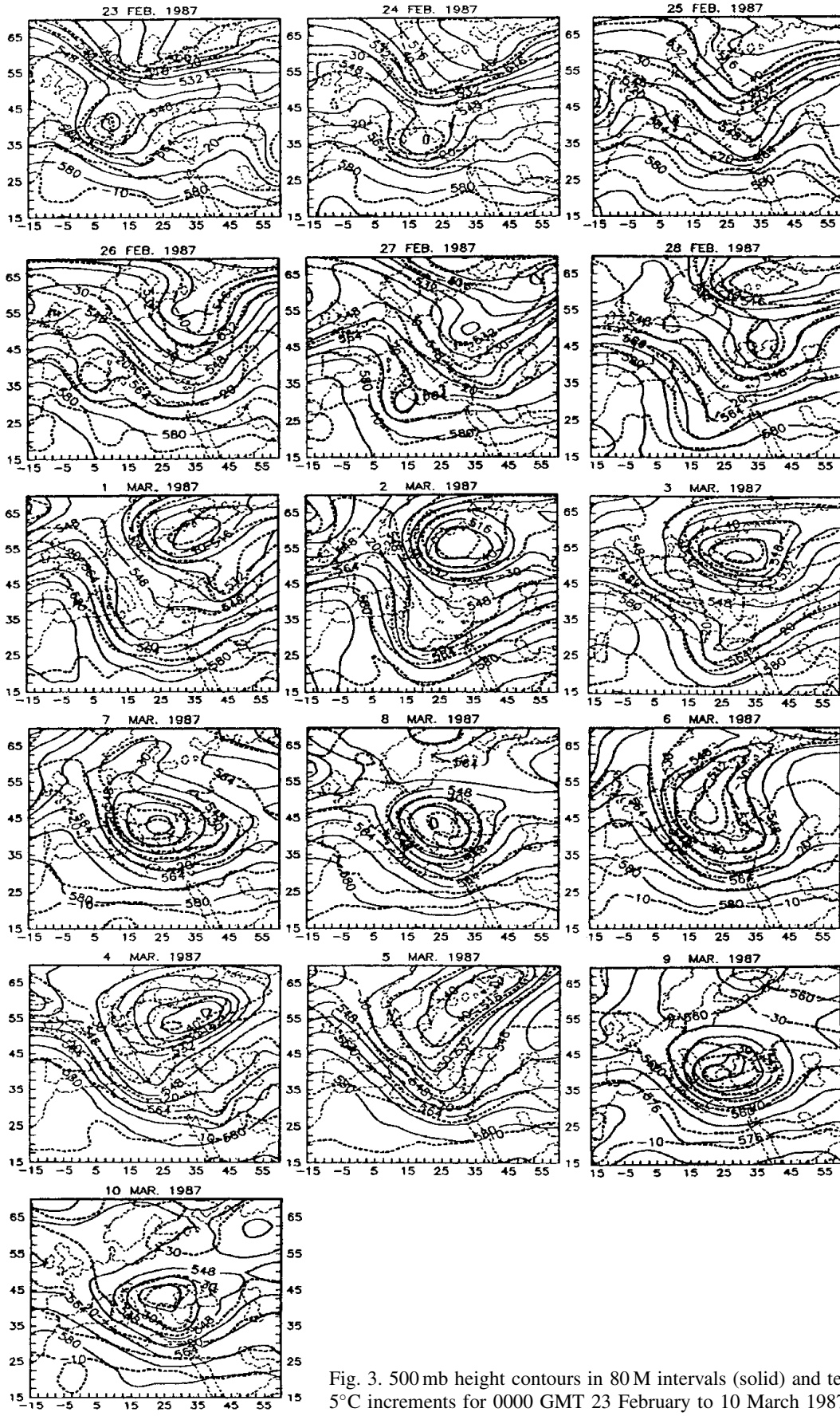

Fig. 3. 500 mb height contours in 80 M intervals (solid) and temperature (dashed) in 5°C increments for 0000 GMT 23 February to 10 March 1987

Upper air charts contain contours of height with 80 meter increment at 500 mb. The surface charts are reproduced by Egyptian Meteorological Authority.

The cyclone of special interest first appeared as an extension of the traveling depression north Europe at 0000 GMT 26 and 27 February a cut-off low formed at 0000 GMT 28 February and a well-defined cyclonic depression become clear over the east of the Paltic sea. The 500 mb trough (Fig. 3) associated with the cyclone is well northwest of Europe by 0000 GMT 28 February, a cut off low at 500 mb was centered over eastern Finland. At 0000 GMT 1 March trough extends from eastern Finland to the western Egypt. A strong thermal gradient lies along the northern Italy and middle of Europe. In this highly baroclinic zone, the surface storm undergoes strong intensification. A closed 500 mb contour developed and moved southeastward at the second day of March where the peak of development exists (Fig. 3).

A drop in the contours of 500 mb level taken place in conjunction with the deepening surface cyclone, and by 0000 GMT 3 March, the 500 mb circulation consists of large cut off low over north Mediterranean. It is also noticed that the horizontal extent of the 500 mb trough is small as inferred from 500 mb hemisphere charts, and the geopotential trough lays behind the thermal trough (Fig. 3) as the tough swings southwest ward to a NE-SW axis. The resulting advection of cold polar air tightens the thermal gradient during the storm intensification. By 28 February the cyclone moved slowly from south to south-westward as it is deepening, and achieving its owest central pressure of 1000 mb to 100 mb 0000 GMT 3 March over north Italy. Twenty-four hours later (Fig. 2), this low pressure has been intensified greater than 5 mb and moved southwest to a point just south of Greece, associated with cold cut-off low in the upper atmosphere. During the next 24 hours the depression started filling and its central pressure increased gradually.

By 000 GMT 5 March the slow-moving ridge of siberian high began to build westward. While the siberian high pressure propagate westward the horizontal extension of the cyclone decrease and moved slowly eastward. The period 6–10 March 1987 (Figs. 2 and 3) is characterized by siberian anticyclone blocking which set up over Europe and it become stationary vortex rotating above the north east of Mediterranean. Such this type of Mediterranean low is called a composite Cyprus low (EL Fandy, 1946). Finally, the cyclone was drifted slowly north-eastward and was cut of the computational domain by 11 March.

5. Analysis of Total Kinetic Energy Budget

5.1 Kinetic Energy Time Development

The energy budget is terms of the Eulerian kinetic energy equation (1) is evaluated in a domain which encloses our cyclone during its life cycle. The area-mean energy variables, integrated from 1000 mb to 100 mb at 0000 GMT are shown in Table 1. Note that the vertical flux divergence was integrated to zero because of the solid boundary condition on ω, therefore, is not presented in Table 1.

5.1.1 Pre-Storm Period

The pre-storm stage of our cyclone, is somewhat unusual since it is affected not only by the entrance of this cyclone from north but also be traveling of another cyclone from the north east of our domain. The generation of kinetic energy term, $-V \cdot \nabla\phi$, shown in Table 1, is negative which indicate on average that the cross contour flow is down gradient the vicinity of the cyclone. The gradual strengthing of the exit of the jet is associated with the traveling depression in the north east corner of the domain which seems to explain the monotonic decrease in horizontal flux convergence after 23 February for the pre-storm stage, and also explain the change of the sign of the rate of change of kinetic energy.

5.1.2 Growth Stage

The kinetic energy increases during the growth period, reaches a maximum at 0000 GMT 2 March. The local variation of kinetic energy, $\partial K/\partial t$, positive throughout most period except during the later portion when the cyclone tend to decay.

Generation of kinetic energy is a prominent sink. The magnitude of this term is evidence of

Table 1. Integrated Kinetic Energy Budget. Unites are W m^{-2} Except for Energy Content which are 10^5 J m^{-2}

Date/Time	K	$\partial K/\partial t$	$-\nabla.kV$	$-V.\nabla\phi$	$D(K)$	$-V.\nabla\phi + D(K)$
Pre-storm period						
23-2/00	9.42	0.40	6.45	−5.44	−0.61	−6.05
24-2/00	10.57	0.46	2.09	−5.20	3.57	−1.63
25-2/00	10.87	−0.45	2.80	−3.62	0.36	−3.26
26-2/00	10.74	−0.24	1.06	−4.99	3.69	−1.30
Growth period						
27-2/00	9.35	0.42	2.41	−23.47	21.48	−1.99
28-2/00	9.97	0.69	6.74	−28.09	22.04	−6.05
1-3/00	11.72	1.89	4.51	−28.17	25.55	−2.62
2-3/00	13.03	0.60	2.59	−24.90	22.91	−1.99
3-3/00	12.99	−1.14	7.15	−11.61	3.32	−8.29
4-3/00	12.16	−0.41	4.93	−3.24	−2.10	−5.34
Decay period						
5-3/00	11.83	−0.04	2.76	5.63	−8.43	−2.80
6-3/00	11.14	−0.46	1.39	1.36	−3.21	−1.85
7-3/00	10.75	−0.80	3.63	4.08	−8.51	−4.43
8-3/00	9.55	−0.42	1.94	−0.10	−2.26	−2.36
9-3/00	9.97	0.07	1.61	1.20	−2.74	−1.54
10-3/00	9.60	0.04	0.92	1.81	−2.69	−1.88
Time Mean	10.85	0.04	3.31	−7.80	4.52	−3.28

widespread and persistent imbalance in the mass and wind fields. The negative values of the generation term on average indicate that the cross contour flow is down gradient in the vicinity of the cyclone. The major source of kinetic energy for the cyclone is due to the horizontal flux convergence. It is the largest component during the growth stage and decreases throughout the development, while it remains positive.

As it is expected, the dissipation $D(K)$ is greatest when the storm is most intensive. An overview of the kinetic energy budget is obtained by comparing the external source or sink $-\nabla \cdot (Vk)$ and the internal source or sink $-V \cdot \nabla\phi + D(k)$ (Chen, 1978). Dissipation of kinetic energy from grid to subgrid scales is an important process during this period. The results in Table 1 reveal that a net transfer of energy from subgrid to grid scales ($D > 0$) is most pronounced during the stage. However, it should be noted that during the growth period positive D values are quite prominent and, in fact, remains a principal source for cyclone.

Table 1 shows clearly that external source dominates during the growth stage. A major contribution from the horizontal flux convergence in this cyclone occurs because the inflow jet is stronger than the out flow one. The gradual strengthening of the inflow jet in the north of the domain seems to explain the nearly increase in horizontal flux convergence.

5.1.3 Decay Stage

The deterioration of the storm system is demonstrated by a steady decrease in kinetic energy. This occurs according to the fact that horizontal transport continuous to represent a major energy source, so this provides a permanent source of energy to the region. Generation of kinetic energy represent another source of energy in this period only, and the dissipation combines to yield an internal sink that exceeds the external source of kinetic energy.

5.2 Time-Height Variations of Budget Quantities

Energetic processes in relation to the cyclogenesis region need further examination and are analyzed by means of time-height cross sections as represented in Fig. 4. The major feature of the cyclogenesis region is the field of kinetic energy due to the persistence of the upper jet stream between 300–200 mb, the maximum value occur during the growth period (Fig. 4). The weakness in the jet start up with the decay period. Systematic changes, related to the life cycle of our case occur in the flux convergence term, this

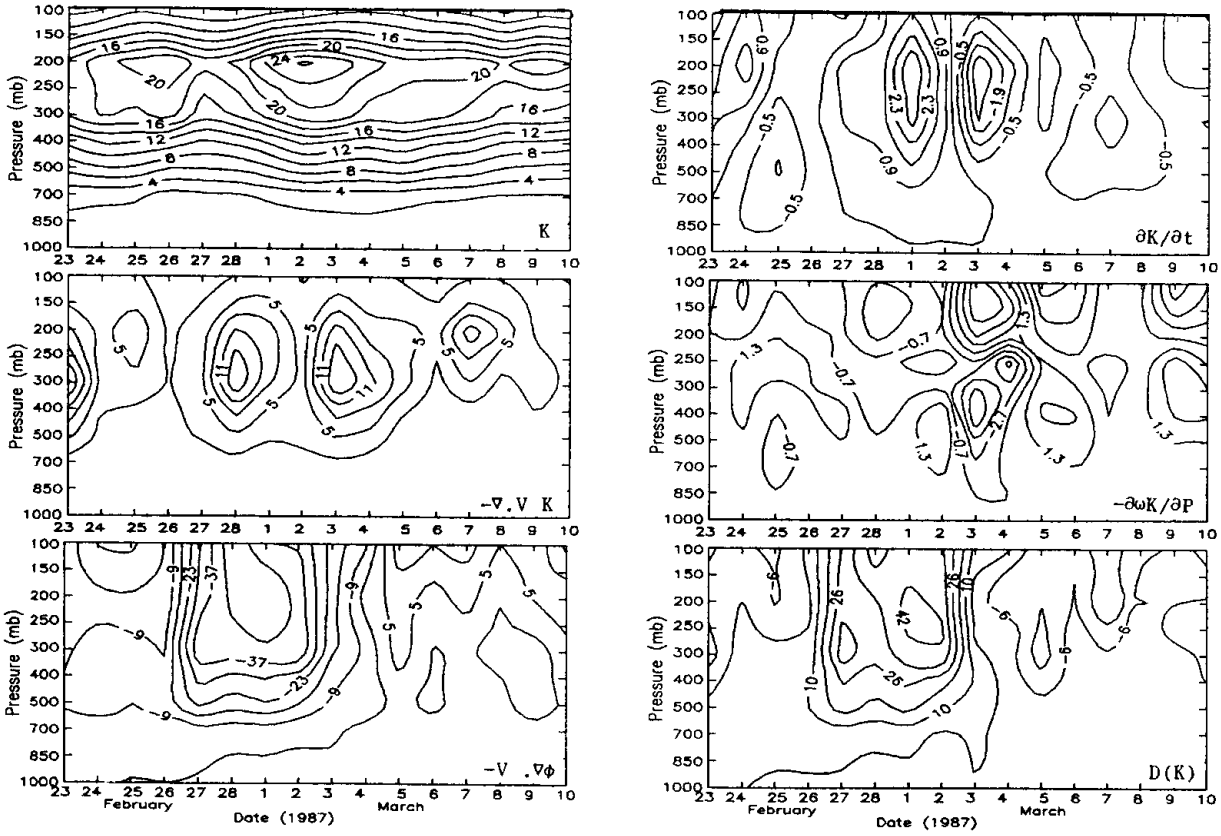

Fig. 4. Pressure-time cross sections of kinetic energy and kinetic energy budget terms. Units: Kinetic energy in $10^5\,\mathrm{Jm}^{-2}$ $(100\,\mathrm{mb})^{-1}$, kinetic energy changes in Wm^{-2} $(100\,\mathrm{mb})^{-1}$

term have positive sign during its three stages and two maximum values in the layer 400–150 mb at 0000 GMT of 28 February and 3 March. So, this term acts as a source of energy specially at the upper levels.

The vertical flux convergence is negative from and above 200 mb which explain the transport of kinetic energy to the stratosphere except at 0000 GMT of 2, 3 and 4 March where the kinetic energy transport is mainly to lower levels. The life cycle of our case study is also well described through generation term $-V \cdot \nabla\phi$. In the growth stage the major energy sink is the intense conversion of kinetic to potential energy by the generation term which reaches its maximum negative value at 000 GMT 1 March and decrease gradually to become positive during the decay period. Here the role of the geopotential fluxes is quantified and provide further breakdown of energy sources in terms of the component $(-V \cdot \nabla\phi)$.

Transfer of kinetic energy from subgrid to larger scales of motion generally is the pronounced feature in our cyclone except at the decay period. Enhanced transfer from subgrid to grid scales of motion is prominent in the middle and upper troposphere and in the lower stratosphere during the growth stage. This term becomes negative and so dissipative losses are now quite prominent during the decay period.

The increase of kinetic energy occurs during the growth stage except at 0000 GMT 3 and 4 March where the negative value becomes clear at the all levels and then extended to the decay period.

5.3 Contribution of Divergent and Nondivergent Wind Components to the Kinetic Energy Budget

5.3.1 Kinetic Energy

In their global study, Chen and Wiin-Nielsen (1976) showed that the kinetic energy K_D of the divergent wind is very small compared to that of the nondivergent wind K_R. However, Chen (1975) noted that K_D may be significant in severe

Table 2. Kinetic Energies K, K_R, K_D and $V_R.V_D$ and the Ratios $K_R/K, K_D/K$ and $V_R.V_D/K$ for Cyclone II. Units: $10^5 \mathrm{Jm}^{-2}$

Date/Time	K	K_R	K_D	$V_R.V_D$	K_R/K	K_D/K	$V_R.V_D/K$
Pre-storm period							
23-2/00	9.42	9.38	0.05	−0.01	99.57%	0.53%	−0.10%
24-2/00	10.57	10.51	0.08	−0.02	99.43%	0.76%	−0.19%
25-2/00	10.87	10.80	0.06	0.01	99.93%	0.55%	0.09%
26-2/00	10.74	10.71	0.04	−0.01	99.72%	0.37%	−0.09%
Growth period							
27-2/00	9.35	9.30	0.06	−0.01	99.46%	0.64%	−0.10%
28-2/00	9.97	9.95	0.06	−0.02	99.79%	0.60%	−0.20%
1-3/00	11.72	11.69	0.04	−0.01	99.74%	0.34%	−0.08%
2-3/00	13.03	13.02	0.07	−0.06	99.92%	0.54%	−0.46%
3-3/00	12.99	12.93	0.07	−0.01	99.53%	0.54%	−0.07%
4-3/00	12.16	12.08	0.10	−0.02	99.34%	0.82%	−0.16%
Decay period							
5-3/00	11.83	11.77	0.05	0.01	99.49%	0.42%	0.08%
6-3/00	11.14	11.07	0.05	0.02	99.37%	0.45%	0.18%
7-3/00	10.75	10.72	0.02	0.01	99.72%	0.19%	0.09%
8-3/00	9.55	9.53	0.04	−0.02	99.79%	0.42%	−0.21%
9-3/00	9.97	9.96	0.04	−0.03	99.89%	0.41%	−0.20%
10-3/00	9.60	9.57	0.04	−0.01	99.68%	0.42%	−0.10%
Time Mean	10.85	10.81	0.05	−0.01	99.63%	0.46%	−0.09%

storms. In Table 2 presentation to the contribution of the divergent and nondivergent wind to the kinetic energy and the ratios $K_R/K, K_D/K$ and $V_R \cdot V_D/K$ for 24 h intervals during the evolution the cyclone. Values of K, K_R and K_D are vary in the same direction while K_R have the major contribution to K. The dot product of the nondivergent and divergent winds $V_R \cdot V_D$ integrates to zero on the glob, but not necessarily in a limited domain. In our case of study term $V_R \cdot V_D$ is smaller than K_D. Values of $V_R \cdot V_D$ are generally smaller than those of K_D, especially in the lower troposphere. The error in approximating K by K_R ranges from 1 to 2% and the average error during the period of cyclone is only about 0.4%. Tim-mean averages of the components of kinetic energies K, K_R, K_D and $V_R \cdot V_D$ and their ratios as a function of pressure for the two cases are expressed in Table 2, pressure time cross-sections of K_R and K_D are also shown in Fig. 5.

K_R remains slightly less than K at all levels except at the lower level (1000 mb) where a maximum contribution of K_R to K occurs. The level of maximum K and K_R (200 mb) coincide with the level of maximum wind. The general decrease in energy appears during the last period of our case.

The cross-sections (Fig. 5) show that the maximum values of K_D are found in the upper troposphere within 300–150 mb layer, these maximum values of K_R are attributed to large horizontal divergent at the jet-stream level which is hypothesized to be induced by the storm outbreak (Maddox et al., 1981) and a Weaker secondary maxima appear in the lower troposphere. Since the rotational wind comprises a large proportion of the total flow, fields of K_R (Fig. 5) closely resemble those of K (Fig. 4).

5.3.2 Horizontal Flux Convergence of Kinetic Energy

The horizontal flux convergence of kinetic energy is regarded as an external energy source and represents the net flow into or out of an open system. The total flux convergence of kinetic energy, $-\nabla \cdot Vk$, may be splited into two parts, one due to the nondivergent wind $-\nabla \cdot V_R k$ and the other to the divergent wind $-\nabla \cdot V_D k$. These quantities at different times in the life cycle of the cyclone are shown in Fig. 7a.

Generally, the values of $-\nabla \cdot V_R k$ closely resemble to those of $-\nabla \cdot Vk$, so neglecting the divergent part of the wind in our case of

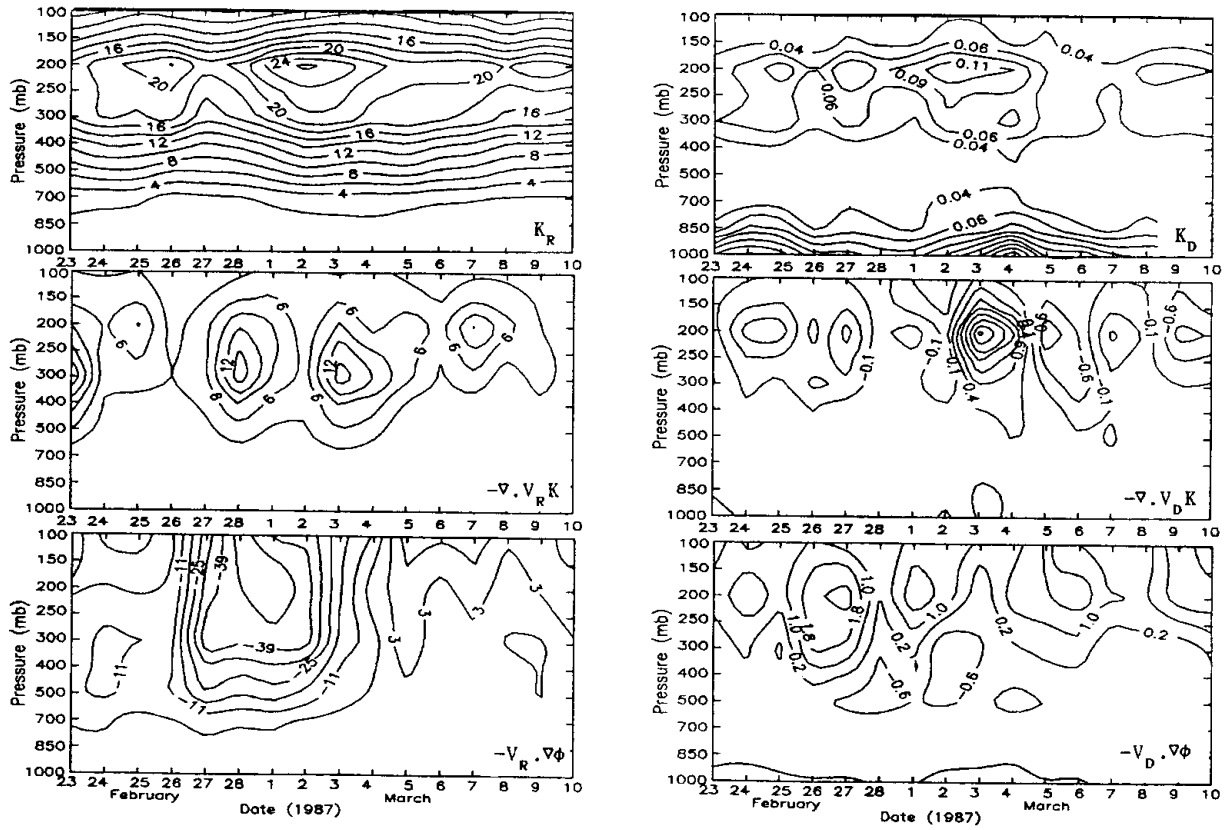

Fig. 5. Pressure-time cross sections of area averaged kinetic energy budget terms. Units of K_D and K_R are $10^5\,\mathrm{Jm}^{-2}$ $(100\,\mathrm{mb})^{-1}$, other units are Wm^{-2} $(100\,\mathrm{mb})^{-1}$

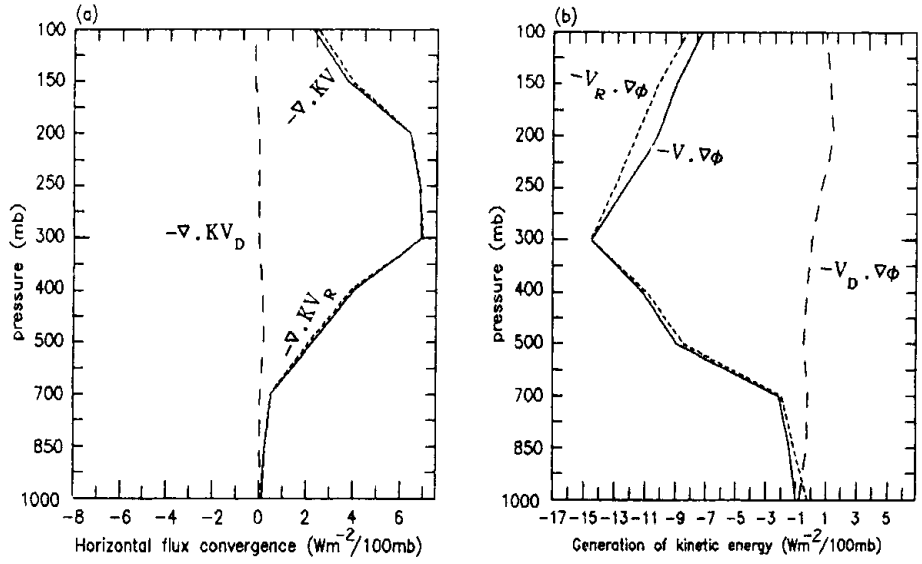

Fig. 6. Time-averged (a) Horizontal flux convergence (b) Generation of kinetic energy by the total wind (solid line), the rotational wind (dotted line) and the divergent wind (dashed line)

study would clearly lead to a very small errors in the calculation of $-\nabla \cdot Vk$. The mean error in the approximation of $-\nabla \cdot Vk$ by $-\nabla \cdot V_R k$ during the life cycle of cyclone is only -1%.

Figure 6a shows the horizontal flux convergence terms with pressure. The rotational wind generally produce inflow of energy at all levels throughout the life cycle of the cyclone (Fig. 6a)

with maximum occurs between 400–150 mb level (Fig. 5). Figure 5,6a show that horizontal import of energy by V_D occurs between 300–150 mb level at 0000 GMT of 28 February 1, 3 and 4 March. The divergent wind produce outflow of energy at the most of the other days.

5.3.3 Generation of Kinetic Energy

The partitioning of kinetic energy generation into baroclinic ($-V_D.\nabla\phi$), and barotropic ($-V_R.\nabla\phi$) parts as in Eq. (6) indicate the generation of kinetic energy at different time steps of development stages for our cases as shown in Fig. 7b. The barotropic contribution $-V_R.\nabla\phi$ is almost negative except at the decay period, this may explain that nondivergent wind blows toward higher pressure most of the time except at the decay stage where the cross-contour flow to divergent wind is predominantly toward lower pressure. The maximum negative values of $-V_R.\nabla\phi$ occurs during the growth stage.

The baroclinic contribution $-V_D.\nabla\phi$ behaves differently when the sign of this term changes several times during the life cycle of the cyclone. Although the magnitude of this term is very small compared to $-V_R.\nabla\phi$ it may be considered as a source of energy for the days with positive sign. The values of $-V_R.\nabla\phi$ it may be considered as a source of energy for the days with positive sign. The values of $-V_R.\nabla\phi$ are closely resemble to those of $-V.\nabla\phi$ so, the average error in approximating $-V_R.\nabla\phi$ by $-V.\nabla\phi$ during the life cycle of the cyclone in the order or -2.8%.

Generation of kinetic energy is shown with the vertical pressure in Fig. 6b. Generation due to barotropic processes predominates at all levels and on the other hand generation due to baroclinic processes is negative below 250 mb and positive from 250 and above on average. Cross-sections (Fig. 5) show that, destruction of kinetic energy by barotropic component is the major sink at all levels throughout the growth period. $-V_R.\nabla\phi$ contributes toward kinetic energy generation during the decay stage. On the other hand the baroclinic component of generation is an energy source above 400 mb, it acts as a sink of energy below this levels in the two cases throughout the life cycle of the cyclone. In his study of a developing baroclinic wave, Krishnamurti (1968) found upper tropospheric cross-contour flow over large areas could be explained by nondivergent wind components. He also observed that the nondivergent wind blows toward higher pressure in the northwesterly current to the rear of the trough and toward lower pressure in the southwesterly flow a head of it. This implies that $-V_R.\nabla\phi$ is negative west of the trough and positive east of it. The negative value of the area-mean of $-V_R.\nabla\phi$ in Fig. 6b is most likely caused by an imbalance between values of $-V_R.\nabla\phi$ on opposite sides of the trough. Hsieh's (1949) provided detailed analysis of cut-off lows mentions a symmetric

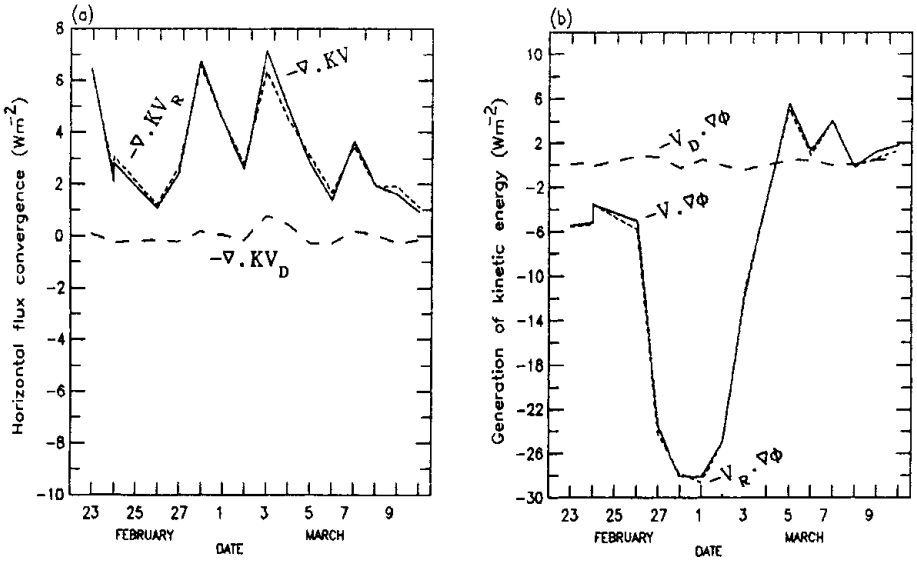

Fig. 7. Vertically averged (a) Horizontal flux convergence (b) Generation of kinetic energy by the total wind (solid line), the rotational wind (dotted line) and the divergent wind (dashed line)

isotach patterns around a trough with stronger north-westerly winds frequently appearing to the west of the trough during cut-off development. The cutoff low decays as the wind field becomes more symmetric about the trough line. The conclusions of Krishnamurti explain the occurrence of negative values of $-V_R.\nabla\phi$ in the upper troposphere of the present study and the approach toward positive values as the storm decays.

6. Results of $\psi.\chi$ Interaction

This part of the present work will focus on the variability of the $\psi.\chi$ interactions during the period of our case study. The energy exchanges are estimated in a domain which encloses the cyclone during its life cycle. Section 6.1 describes the development of the four leading terms of the $\psi.\chi$ interactions. Section 6.2 studies the time-height variations of the $\psi.\chi$ interactions terms while Sect 6.3 is concerned with the study of spatial distribution of the first term of the $\psi.\chi$ interactions for some days in the used period.

6.1 Time Development of $\psi.\chi$ Interaction

Area-averaged, vertically integrated $\psi.\chi$ interaction terms for the period of the two cyclones are presented in Fig. 8.

The first term $\overline{\overline{f\nabla\psi\cdot\nabla_\chi}}$ depends on the orientation of $\nabla\psi$ and $\nabla\chi$ and turned out to be the leading one among the interaction terms. Figure 8a shows that this term is positive throughout the period (23 February to 10 March) which means that during this period the non-divergent motions associated with the cyclone receive energy from the divergent circulation. This feature persists throughout the period and is stronger generally in the growth period of the cyclone. The behaviour of this term found to be consistent with the behaviour of kinetic energy (Table 1) of the cyclone and also the maximum of energy exchanges from the irrotational to the nondivergent modes specially at 2 March.

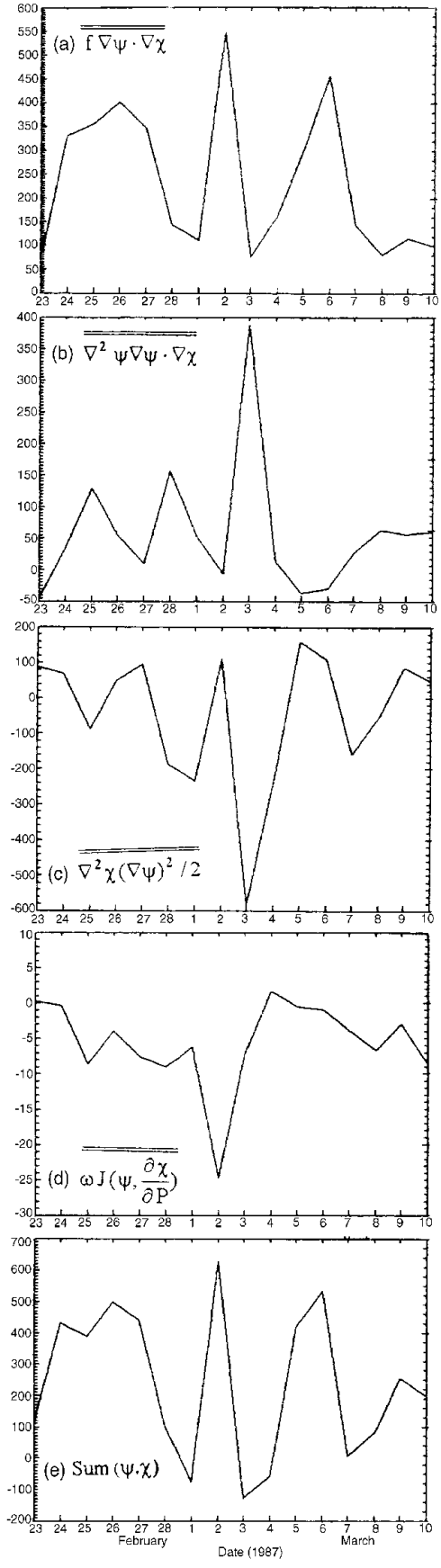

Fig. 8. Time variation of the different terms of $\psi\cdot\chi$ interactions over the domain of computation. Units $10^{-6}\,m^2\,s^{-3}$

The second term $\overline{\overline{\nabla^2\psi\nabla\psi\cdot\nabla_\chi}}$ has a positive sign for most days within the computational domain. The sign is related to the fact that the current within this domain has a positive relative vorticity. The magnitude of this terms is of the order of $+40\times10^{-6}\,\mathrm{m^2\,s^{-3}}$ and making as the first term in converting energy from irrotational to the nondivergent modes. The maximum values of this term occurs at 25, 28 February and 3 March.

The sign of the third term $\overline{\overline{\nabla^2\chi(\nabla\psi)/2}}$ (Fig. 8c) depends upon the existence of convergence ($\nabla^2\chi>0$) or divergence ($\nabla^2\chi>0$) over our domain of computation. Figure 8c show that there are transfer of energy to divergent flow at nine days and energy exchange from irrotational to nondivergent flow occurs at the rest of days of out period. The mean value of this term ($-19\times10^{-6}\,\mathrm{m^2\,s^{-3}}$) indicates that a transfer of energy to divergent component occurs by the third term throughout the period of study. The maximum total values of this transfer ($-1037\times10^{-6}\,\mathrm{m^2\,s^{-3}}$) appear in the growth period with greatest one ($-583\times10^{-6}\,\mathrm{m^2\,s^{-3}}$) at 3 March.

Figure 8d illustrates the last term $\omega J(\psi,\frac{\partial\chi}{\partial P})$ of the transfer of energy to irrotational component occurs throughout the period of study except at 23 February and 4 March. This term exhibit a sharp increase of its negative values at 2 March. However the last term can be neglected when comparing its magnitude with the other terms.

Order of magnitude of our calculations show that the leading terms among these are the first two terms which depends upon the orientation of $\nabla\psi$ and $\nabla\chi$ and the third term that lead to an exponential growth of nondivergent kinetic energy wherever $\nabla^2\chi>0$.

Since the first term $f\nabla\psi.\nabla\chi$ is the largest term the behaviour of the sum of the of $\psi.\chi$ interaction terms (Fig. 8e) is somewhat coincide with the behaviour of the first one. On the other hand Fig. 8e illustrates the energy exchange from irrotational to nondivergent flows throughout the period except at three days only (1, 3 and 4 March).

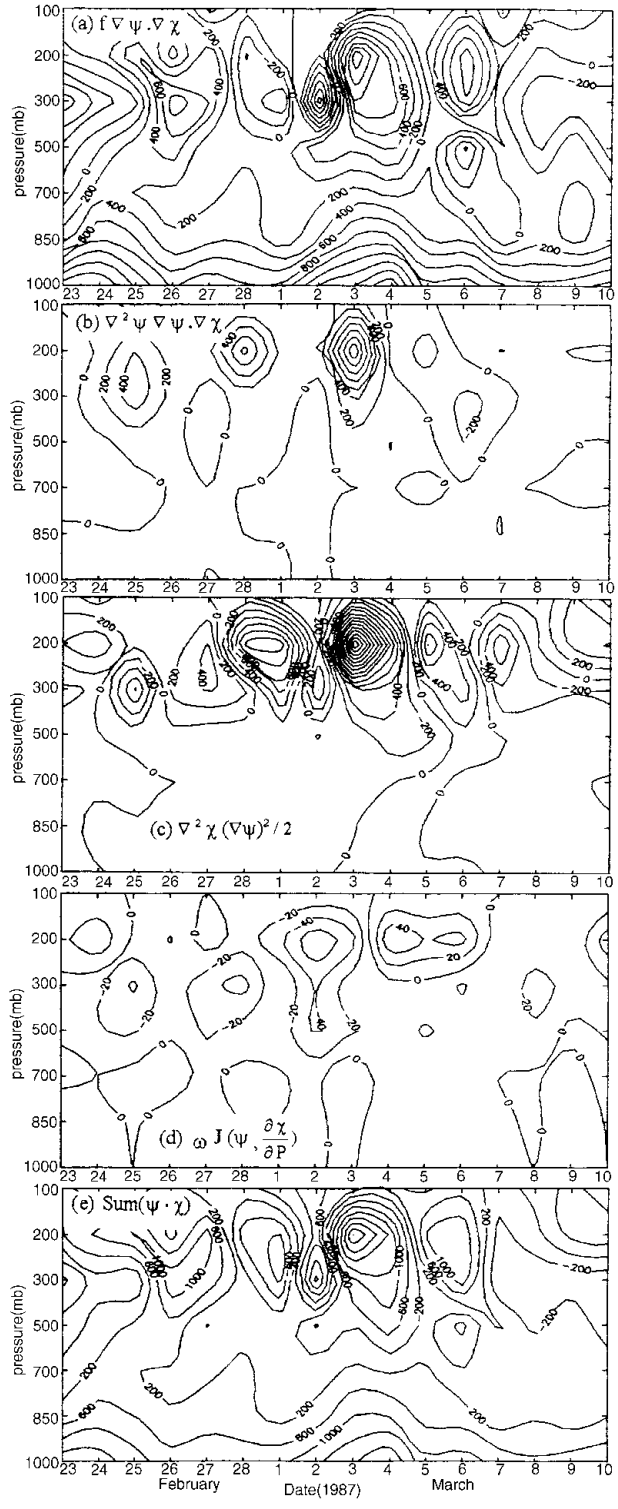

Fig. 9. Time-height variation of the different terms of $\psi\cdot\chi$ interactions over the domain of computation

6.2 Time Height Variation of $\psi.\chi$ Interaction

Energy exchanges in relation to the cyclogenesis region need further examination, so, here we shall illustrate the time-height history of the four leading terms of the $\psi.\chi$ interactions.

Figure 9a shows that the major feature for the first term is the persistence of the energy

exchange from irrotational to nondivergent flow below 700 mb. This energy exchange increase gradually from 700 mb to 1000 mb with a maximums appears at 24 February and 3, 4 March. The most striking feature is the persistence of the transport of energy from divergent to nondivergent flow at all levels during the period 25–28 February. Another but strong exchange from irrotational to nondivergent flow appears above 300 mb at the days 2 and 6 March.

Figure 9b illustrates that the values of the second term below 500 mb are very small throughout the period of the cyclone and so the role of this term in energy exchange can be neglected below 500 mb. It is interesting to note that the most maximum values exists between 300 and 200 mb levels.

During the period from 24 February to 4 March and above 500 mb it is clear that energy exchange from irrotational to nondivergent flow may be noted with largest three maximum one at 25 February (300 mb), another at 28 February (200 mb) and the third which is the greatest one at 3 March (200 mb). Transfer of energy to the divergent component at 200 and 300 mb occurs at days 23 February and 2, 5, 6 March.

As in case of the second term the contribution of the third term below 500 mb level (Fig. 9c) to the energy exchange is very small with respect to the first term and so it can be neglected. The most striking features for this term appears at the days 28, 1, 2, 3, 4 and 5 March where a sharp changes in the interaction can be easy observed at 200 and 300 mb levels. While a large amount of energy transfer to the irrotational component at 28, 1, 3 and 4 March, a less amount of energy exchange from irrotational to nondivergent one at 2 and 5 March.

Although the contribution of the last term, $\omega J(\psi, \partial\chi/\partial P)$, to the $\psi.\chi$ interactions may be neglected Fig. 9d illustrates very small energy exchange by this term at the upper levels above 500 mb, and the transfer of energy to the divergent component appears at the most days.

Figure 9e shows time-height variation of the sum of the four leading terms of the $\psi.\chi$ interaction. It is clear that the first term is a dominant one below 700 mb which means that energy exchanges from irrotational to nondivergent components occurs only by the first term. Another point to be noticed from Fig. 9e is that in the upper troposphere important fluctuation in the magnitudes of $\psi.\chi$ interactions occur due to the different contributions of the first three terms. The contribution of the last term may be considered as the smallest one.

6.3 The Spatial Distribution of a Selected Period

This section is concerned with the study of the spatial distribution of the first term (largest one) of the j.c interaction for the period from 28 February to 5 March where a sharp changes in the $\psi.\chi$ interaction may be exist. Figure 10a, 10c illustrate the fields of ψ, χ and $f\nabla\psi.\nabla\chi$ during this period at 300 and 200 mb levels. The comparison between the evolution of ψ,χ and $f\nabla\psi.\nabla\chi$ during the different days in this period can be summarized as follows:

1. Generally, the ψ, χ isopleths show a preferred orientation (Fig. 10a, b) and as may be seen in Fig. 10c a distinct maxima in $f\nabla\psi.\nabla\chi$ are observed over our domain throughout this period.

2. Figure 10c, 28 February, illustrates the first indication of significant energy exchange from the divergent over the east of Mediterranean where the first term over this area at 200 mb is large, and the ψ, χ isopleths acquired a south-west-northeast orientation over most of this area where the trough associated with the cyclone is well northeast of Europe and a cut off low at 500 mb (Fig. 3) was centered over eastern Finland.

3. The most striking feature is the existence of a two main active areas of energy exchanges at 1 March (200 mb), the first one extended from north Spain to north Libya and the second extended from north Egypt to northeast of Turkey. Above the second area the divergent circulation transfer substantial amounts of energy to the nondivergent circulations while above the first area transfers to divergent one are quite large, this feature of less intense appears on 300 mb level. Maps of circulations during this day show that the depression moved southwest ward.

4. With the movement of depression southwest ward at 2 March, the fields of ψ, χ and $f\nabla\psi.\nabla\chi$ exhibited an interesting evolution over our domain, where the second active area (200 mb) moved westward and the first one moved east-

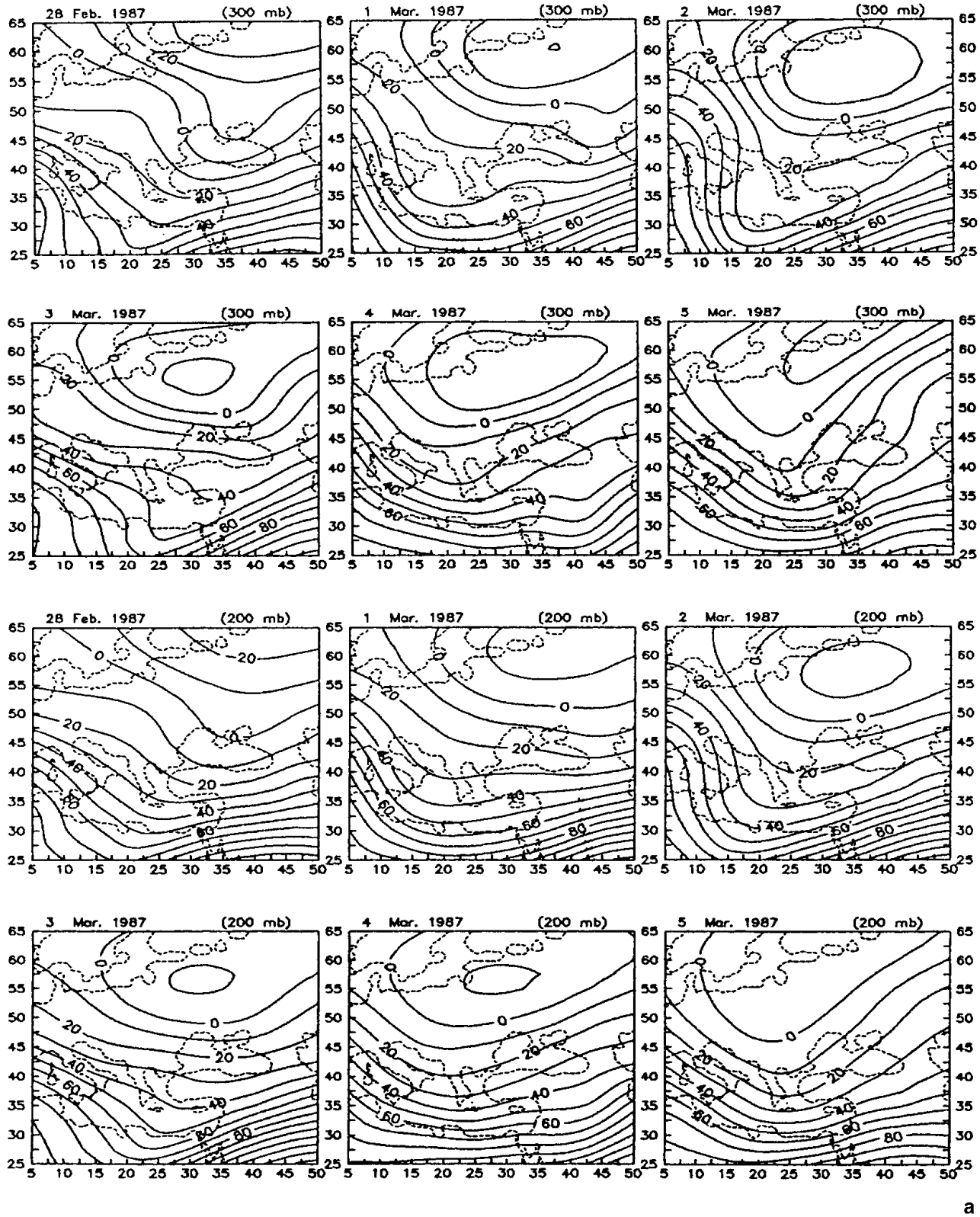

Fig. 10a. Charts of the stream function ψ for the selected period (28 February to 5 March)

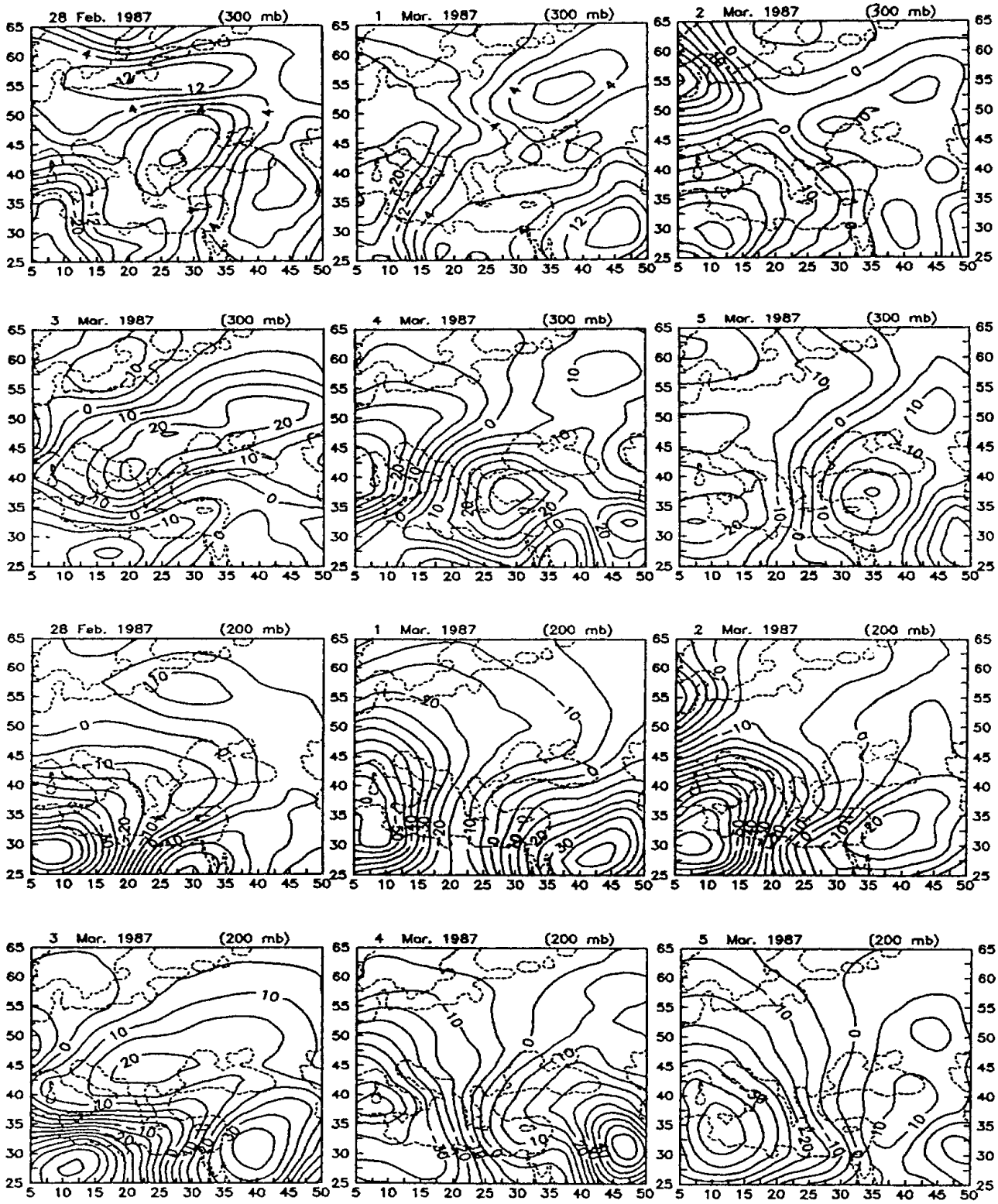

Fig. 10b. Charts of the velocity potential χ for the selected period (28 February to 5 March)

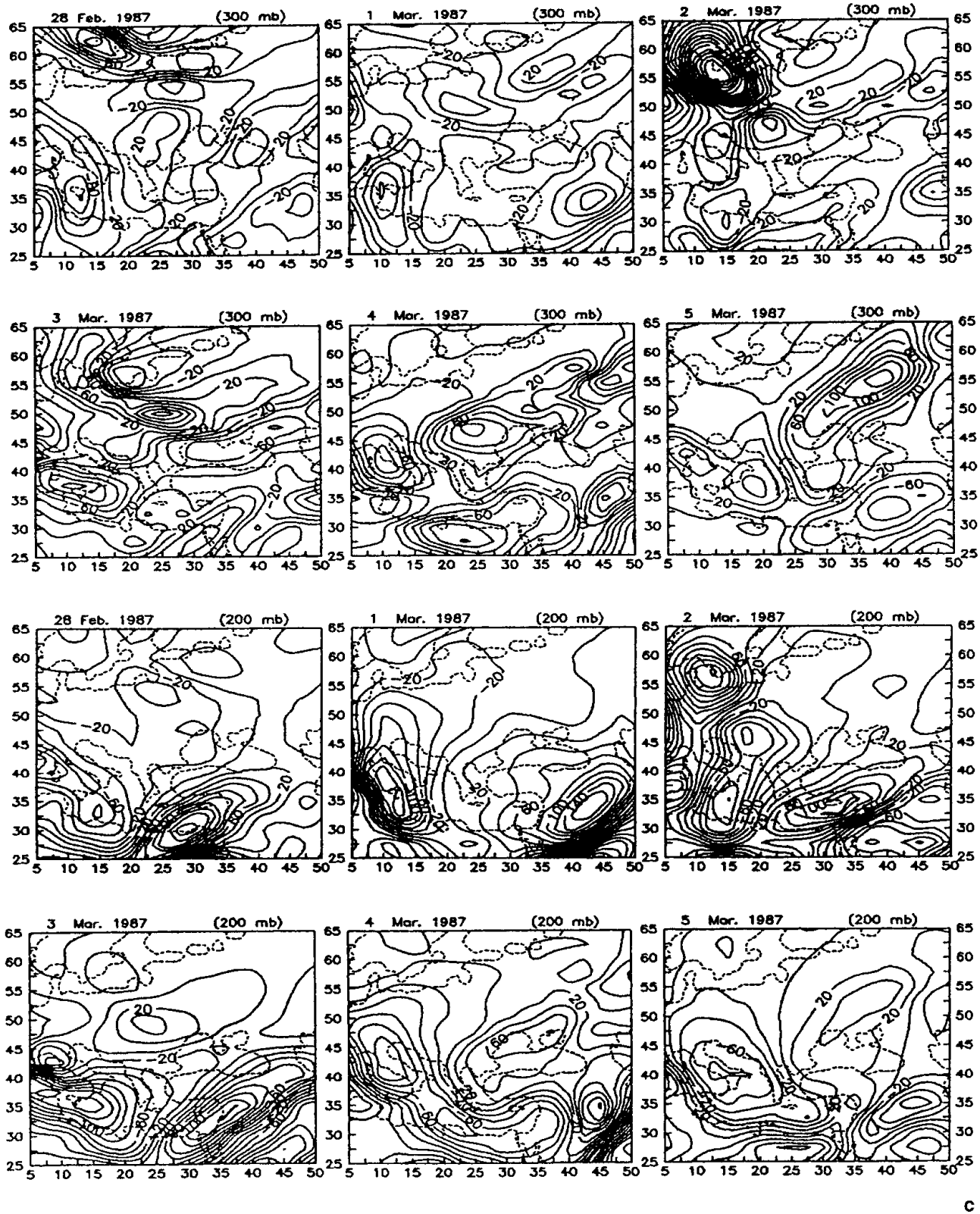

Fig. 10c. Charts of $f\,\nabla\psi\cdot\nabla\chi$ for the selected period (28 February to 5 March)

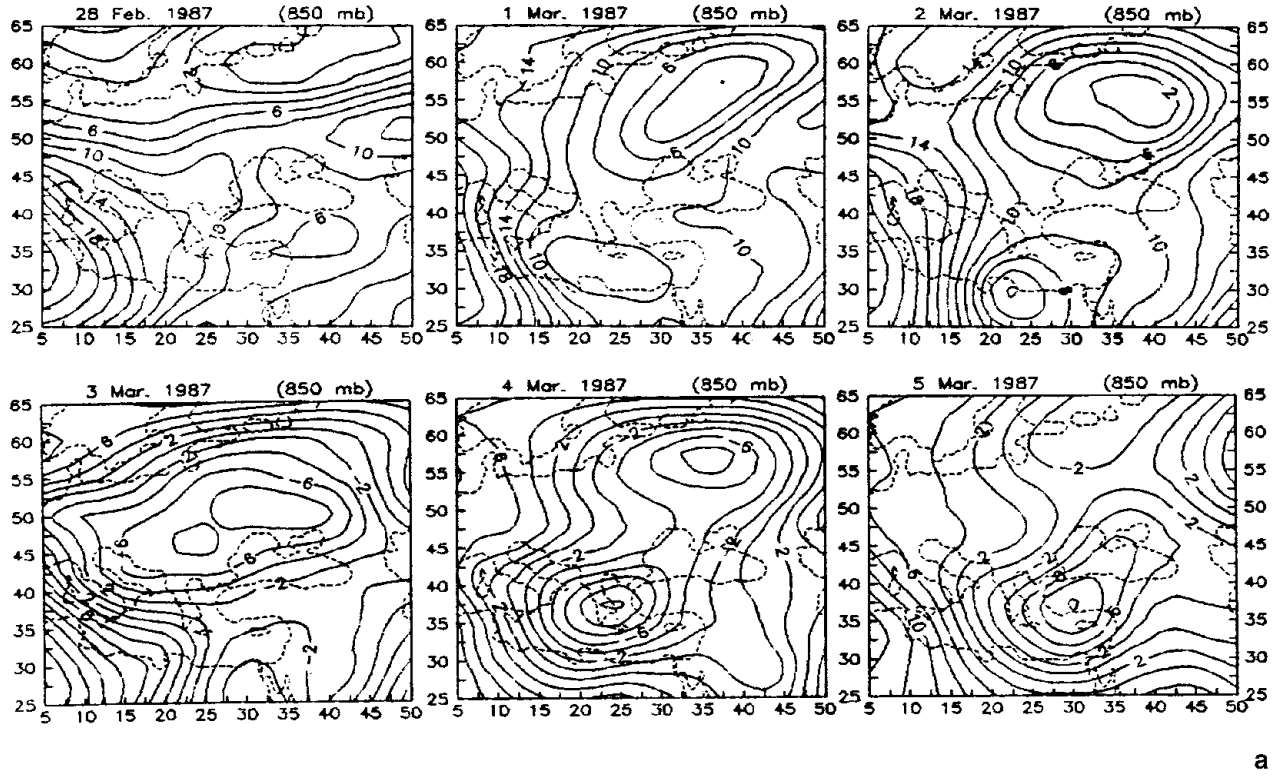

Fig. 11a. The same as Fig. 10 a but for 850 mb

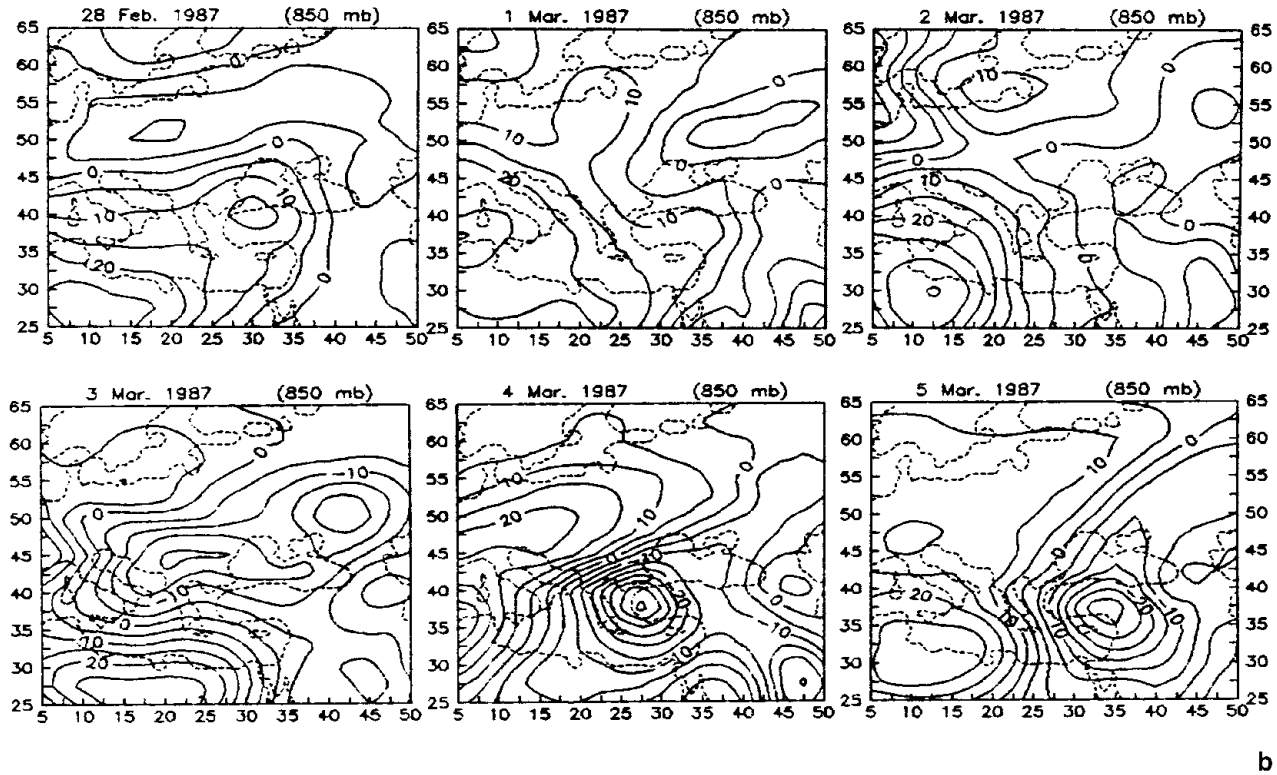

Fig. 11b. The same as Fig. 10 b but for 850 mb

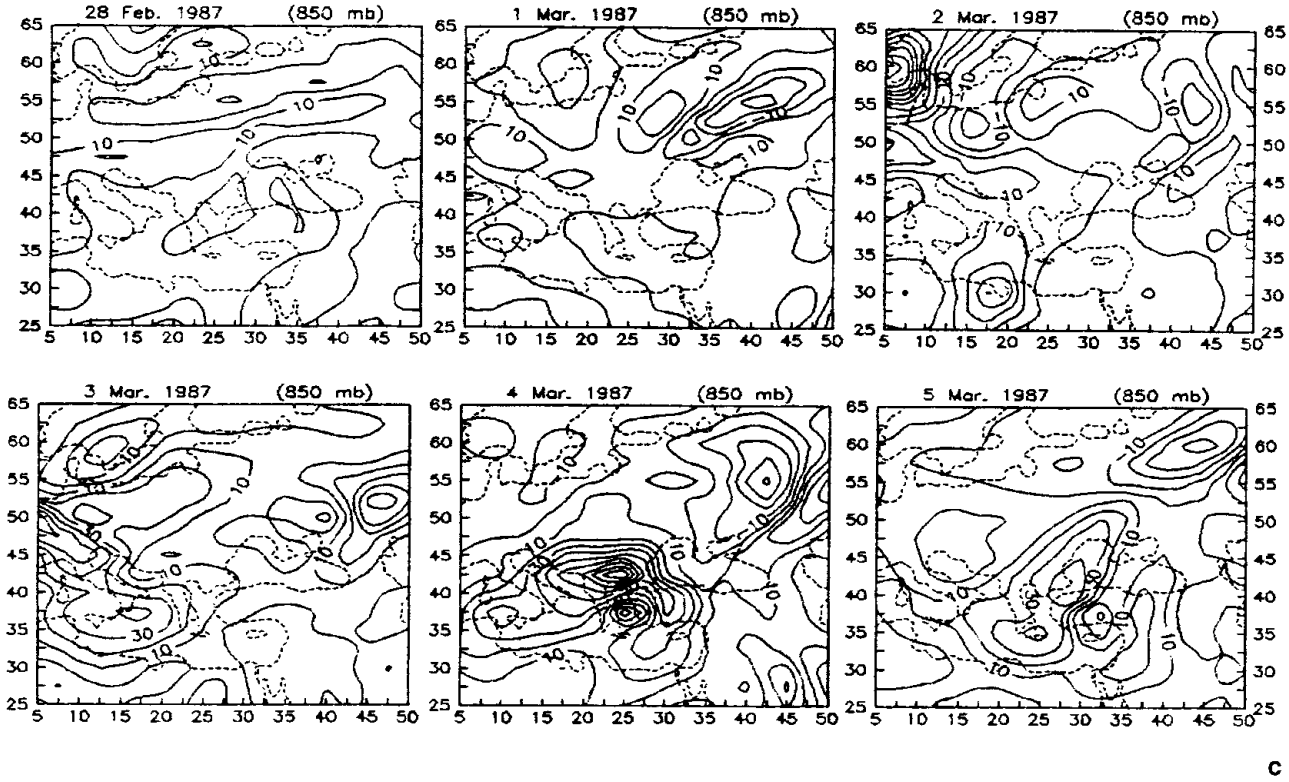

Fig. 11c. The same as Fig. 10 c but for 850 mb

ward. It is of interest to note that the orientation of ψ and χ isopleths over the northwest of our domain provides a favorable orientation for the $\nabla\psi$ and $\nabla\chi$ vectors over this area and a substantial exchange of energy from the irrotational to the divergent motion occurs at 300 and 200 mb levels.

5. At the third of march the orientation of $\nabla\psi$ and $\nabla\chi$ over the northwest of out domain changes and become not favorable for the transfers of energy. On the other hand the second main active area moves slowly eastward while the first one becomes zonal. On the vertically averaged sense the transfer of energy to the nondivergent component is less than the other days.

6. During the 4 and 5 of March another change in the orientation of the ψ, χ isopleths occurred. The ψ isopleths acquired northwest-southeast orientation over our domain, thus rendering $\nabla\psi.\nabla\chi$ to be smaller than other days at 300 and 200 mb levels, and the position of two main active areas changes. The second area which have $f\nabla\psi.\nabla\chi>0$ will become very small.

7. Throughout this period the prominent streamfunction maximums was present southeast of the Mediterranean. Both $\nabla\psi$ and $\nabla\chi$ are nearly parallel and a large contribution to the exchange from irrotational to the nondivergent flows occurs which indicate that the subtropical jet steadily receives energy from divergent flow.

8. The subtropical jet over the southeast of Mediterranean exhibits a preferred orientation of $\nabla\psi$ and $\nabla\chi$ and receives energy from the divergent circulations. A careful inspection of the charts of this period and the corresponding charts of kinetic energy show that this feature remains associated with the jet appears and the energy changes of $f\nabla\psi.\nabla\chi$ is also important aspect of the dynamics of the subtropical jet.

9. For pure nondivergent barotropic dynamics the interaction term $f\nabla\psi.\nabla\chi$ is identically zero for a closed domain, thus it appears that one cannot rule out baroclinic effects in the dynamics of this depression.

7. Concluding Remarks

This paper has described the kinetic energy budget and the relative contributions of divergent and rotational wind components to the kinetic energy balance during the period of a Mediterranean cyclone. The most significant findings are as follows:

1. Horizontal flux convergence constitutes may act as a major energy source. Generation of kinetic energy via cross-contour flow is, surprisingly, a persistent sink except only a weak energy source for the decay period. Negative generation results from strong flow propagating into regions of weaker pressure gradients a head of upper air troughs.

2. Dissipation of kinetic energy has two local maxima one in the lower troposphere (nearly balancing the generation term) and second located near the jet stream level. Subgrid-scale sources of kinetic energy are apparent and, at times, are particularly important in regions of deep cyclogensis. The balance of source and sink terms is basically similar with maximum generation and dissipation in the lower troposphere and at the jet stream level.

3. Temporal variations in the generation term flux convergence and dissipation terms of kinetic energy budget are related to the life cylces of the cyclone. Maximum energy conversion and transport occur near the time of maximum storm intensity while smaller values are observed during the development and decay stages.

4. The major contribution to kinetic energy comes from a persistent upper tropospheric jet stream activity throughout the period of the cylcone. Most of this energy occurred above 400 mb in association with the strong jet stream.

5. V_D contributes 1–2% of the total kinetic energy but nearly 1–4% of the flux convergence of total kinetic energy during the lifetime of the cyclone. So, in calculating the magnitude of kinetic energy, one may safely replace the total wind with the nondivergent wind.

6. The generation of kinetic energy by baroclinic processes, $-V_D.\nabla\phi$ is $0.22\,\mathrm{wm}^{-2}$ while for barotropic processes, $-V_R.\nabla\phi$ is $-8.02\,\mathrm{wm}^{-2}$ averaged over the life time of the cyclone.

This study has emphasized and pointed out also the role of the energy exchanges from the irrotational to the nondivergent component during the period of study. The main results can be summarized as follows:

a. The first term $f\nabla\psi.\nabla\chi$ may be considered as the leading one among the interaction terms. Throughout our period this term makes to transfer of energy from the irrotational component to the nondivergent one specially in the lower levels.

b. The role of the second and third terms in energy exchanges is less important than the first one, while the last term can be neglected when comparing its magnitude with the other terms. Although the contribution of the second and third terms to the sum is very small at the lower levels this contribution is large at the upper levels specially at 300 and 200 hPa level

c. The fields of the first term at 200hPa level show that the orientation of the two active areas of energy exchanges are associated with the movement of the cyclone.

d. A large increase in the kinetic energy of the total flow fields and the nondivergent component of the flows occurs over southeast of Mediterranean with the existence of the subtropical jet this indicate that the subtropical jet steadily receives energy from divergent flow. A careful inspection of the charts of this period and the corresponding charts of kinetic energy show that this feature remains associated with the jet appears and the energy changes $f\nabla\psi.\nabla\chi$ is also important aspect of the dynamics of the subtropical jet.

e. Most of total kinetic energy is in the nondivergent component and a large proportion of this must come from the irrotational component thus barotropic energy exchanges and barotropic instability may yet require that the $\psi.\chi$ interactions supply energy to the basic flow steadily.

f. The kinetic energy of the divergent circulation does not increase much with time. This energy is shown to be transferred rapidly to the nondivergent motion via a number of interaction function.

Acknowledgements

The authors are indebted to Professor T. N. Krishnamurti Florida State University Department of Meteorology for his helpful suggestions and support of this work.

References

Chen, T.C., 1975: On the kinetic energy of the divergent and nondivergent flow in the atmosphere. Tech. Rep. 02630-14-T, Dept. Atmos. Oceanic Sci., University of Michigan, 143 pp.

Chen, T.C., 1980: On the energy exchange between the divergent and rotational components of atmospheric flow over the tropics and subtropics at 200 hPa during two northern summers. *Mon. Wea. Rev.*, **108**, 896–912.

Chen, T.C., Wiin-Nielsen, A., 1976: On the kinetic energy of the divergent and nondivergent flow in the atmosphere. *Tellus*, **28**, 486–498.

Chen, T.C., Alpert, J. C., Schlatter, T. W., 1978: The effects of divergent and nondivergent winds on the kinetic energy budget of a midlatitude cyclone: A case study. *Mon. Wea. Rev.*, **106**, 458–468.

DiMego, G. J., Bosart, L. F., 1982: The transformation of Tropical Storm Agens into an extratropical cyclone. Part II: Moisture, voriticity and kinetic energy budgets. *Mon. Wea. Rev.*, **110**, 412–433.

EL-Fandy, M. G., 1946: Baroclinic low Cyprus. *Quart. J. Roy. Meteor. Soc.,* **72**, 291–306.

Fuelberg, H. E., Jedlovec, G. J., 1982: A subsynoptic-scale kinetic energy analysis of the Red River Valley tornado outbreak (AVESESAME I). *Mon. Wea. Rev.*, **110**, 2005–2024.

Fuelberg, H. E., Scoggins, J. R., 1978: Kinetic energy budgets during the life cycle of intense convective activity. *Mon. Wea. Rev.*, **106**, 637–653.

Holopainen, E., 1973: An attempt to determine the effects of turbulent friction in the upper troposphere from the balance requirements of the large-scale flow: A frustrating experiment. *Geophysica*, **12**, 151–176.

Hsieh, Y. P., 1949: An investigation of a selected cold vortex over North America, *J. Meteor.*, **6**, 401–410.

Krishnamurti, T. N., 1968: A study of a developing wave cyclone. *Mon. Wea. Rev.*, **96**, 208–217.

Krishnamurti, T. N., 1971: Observational study of the tropical upper tropospheric motion field during the Northern Hemispheric summer. *J. Appl. Meteor.*, **10**, 1066–1096.

Krishnamurti, T. N., Bounoua, L., 1996: *An Introduction to Numerical Weather Prediction Techniques*. New York: Academic Press, pp. 73–76.

Krishnamurti, T. N., Ramanathan, Y., 1982: Sensitivity of the monsoon onset to differential heating. *J. Atmos. Sci.*, **39**, 1290–1306.

Kung, E. C., 1966: Kinetic energy generation and dissipation in the large scale atmospheric circulation. *Mon. Wea. Rev.*, **94**, 67–82.

Kung, E. C., 1969: Further study on the kinetic energy balance. *Mon. Wea. Rev.*, **97**, 573–581.

Kung, E. C., Tsui, T. L., 1975: Subsynoptic-scale balance in the storm area. *J. Atmos. Sci.*, **32**, 729–740.

Maddox, R. A., Perkey, D. J., Fritsch, J. M., 1981: The evolution of upper tropospheric features during the development of a midlatitude mesoscale convective complex. *J. Atmos. Sci.*, **38**, 1664–1674.

McInnis, D. H., Kung, E. C., 1972: A study of subsynoptic-scale energy transformations. *Mon. Wea. Rev.*, **100**, 126–13.

O'Brien, J. J., 1970: Alternative solutions to the classical vertical velocity problem. *J. Appl. Meteor.*, **9**, 197–203.

Pearce, R. P., 1974: The design and interpretation of diagnostic studies of synoptic-scale atmospheric systems. *Quart. J. Roy. Meteor. Soc.*, **100**, 265–285.

Robertson, F. R., Smith. P. J., 1980: The kinetic energy budgets of two severe strom producing extratropical cyclones. *Mon. Wea. Rev.*, **108**, 127–143.

Smith, P. J., Adhikary, S. P., 1974: The dissipation of kinetic energy in large-scale atmospheric circulations. *Rev. Geophys. Space Phys.*, **12**, 281–284.

Tsui, T. L., Kung, E. C., 1977: Subsynoptics-scale energy transformations in mvarious severe storm situations. *J. Atmos. Sci.*, **34**, 98–110.

Vincont, D. G., Schlatter, T. W., 1979: Evidence of deep convection as a msource of synoptic-scale kinetic energy. *Tellus*, **31**, 493–504.

Author's addresses: M. Abdel Wahab, Department of Astronomy and Meteorology, Faculty of Science, Cairo University, Cairo, Egypt; H. Abdel Basset, Department of Astronomy and Meteorology, Faculty of Science, Al-Azhar University, Nasr City, Cairo, Egypt.